coatings

MDPI

Article

Sliding Wear Behavior of Fe-Al Coatings at High Temperatures

Núria Cinca [1,*], Slawomir Cygan [2], Cezary Senderowski [3], Lucyna Jaworska [2], Sergi Dosta [1], Irene G. Cano [1] and Josep M. Guilemany [1]

1 Centre de Projecció Tèrmica (CPT), Departament de Ciència dels Materials i Química Física, Universitat de Barcelona, 08028 Barcelona, Spain; sdosta@cptub.eu (S.D.); igcano@cptub.eu (I.G.C.); jmguilemany@cptub.eu (J.M.G.)

2 Centre for Materials Research and Sintering Technology, Institute of Advanced Manufacturing Technology, 30-011 Krakow, Poland; slawomir.cygan@ios.krakow.pl (S.C.); lucyna.jaworska@ios.krakow.pl (L.J.)

3 Department of Materials Technology and Machinery, University of Warmia and Mazury, 10-719 Olsztyn, Poland; cezary.senderowski@uwm.edu.pl

* Correspondence: ncincacpt2@gmail.com; Tel.: +34-93-402-12-97

Received: 23 June 2018; Accepted: 26 July 2018; Published: 31 July 2018

Abstract: The medium and high temperature tribological behavior of different iron aluminide thermal spray coatings was investigated. Several powders synthesized through different routes (ball milling, self-decomposition, and self-propagating high-temperature sintering (SHS)) were evaluated. High heterogeneity of conventional High Velocity Oxygen Fuel (HVOF) coatings plays a vital role in their sliding performance, but as long as their integrity is preserved under high temperature oxidizing conditions, the wear rates are found to be acceptable, as it occurs in the case of ball milled Fe-40Al (at.%) powder. The friction phenomenon and wear mechanisms were analyzed in detail through the wear track morphology, contact surface, and friction coefficients. The occurrence of brittle phases in the sprayed coatings, which are also present when tested at high temperatures, appeared to be crucial in accelerating the coating failure.

Keywords: intermetallics; coatings; wear

1. Introduction

Intermetallic compounds (IMCs) that are based on Ni and Fe aluminides are potentially applicable at moderate and high temperatures [1,2] due to their ability to form protective alumina layers that make them excellent candidates for withstanding oxidation, sulfidizing, and carburizing atmospheres, even at temperatures as high as 1000 °C [3]. Possible applications of such coatings can be found in the gas turbine engine industry for commercial and military aircraft, industrial power generation, and marine applications. There is also an increasing interest in their use for wear resistance [4–6]; their performance as matrix with the reinforcement of ceramic particles was compared to WC-Co hard metals [7–14].

Iron aluminides, mainly FeAl and Fe_3Al, have recently aroused special technological interest recently. Alman et al. [8,9] reported that the erosion rates of the FeAl-based cermets tend to decrease or remain constant when the test temperature is increased, whereas the erosion rates of the WC-Co alloy continually increase under conditions of elevated temperatures. By comparing the wear resistance of iron aluminide alloys to those of other ceramics and metals, the above-mentioned authors observed that the resistance of iron aluminides had similar magnitudes to those of austenitic stainless steels. In addition, by increasing the Al content, the wear rate decreased more than that of the bulk hardness. The sliding wear performance was also examined under several contact conditions

against different counterpart materials i.e., AISI52100 bearing steel [14], Al_2O_3 [4], WC-Co [5], and Si_3N_4 [12]. Wear resistant materials at elevated temperatures are needed in a large selection of industrial applications, such as high temperature bearings, transport, materials processing, etc. [15,16].

Therefore, the high temperature wear performance of intermetallic aluminides may be of interest in a number of components. Even though they show good strength and environmental stability, several defects were detected, such as poor ductility and toughness at room temperature, mediocre creep strength, as well as fabrication difficulties. Such deficiencies impose a great concern for their application as industrial structural materials [17,18], and several routes are proposed to improve it, i.e., (i) addition of alloying elements; (ii) reduction in grain size; (iii) disordering of the lattice, to improve the dislocation motion; and, (iv) modifying the crystal structure of the phase into a more symmetric; some of these effects can be achieved by mechanical alloying/milling [19,20].

Therefore, they emerged as interesting materials for coatings to protect more conventional higher-strength materials. Several deposition techniques were investigated to synthesize aluminide coatings, such as weld overlay, pack cementation, electro-spark deposition (ESD), magnetron sputter deposition, and thermal spray techniques [21–31].

Some authors have already investigated thermal sprayed intermetallic coatings for wear applications [21–31]. In those previous studies, Plasma Spraying (PS) and High Velocity Oxygen Fuel (HVOF) processes were mainly employed by using different feedstock composition. It is well known that the proper selection of nominal composition can have an effect the deposition behavior as well as the it is a posteriori performance; for example, Cr, Zr, and B were among the alloying elements extensively studied [25,32], with great emphasis placed upon the effects on the mechanical and oxidation properties of Fe-Al alloys at different temperatures. In addition, the role of the powder manufacturing route also results in a different coating microstructure, and, therefore, changes on in the properties, due to deviations from precise stoichiometry in either one side of the nominal atomic ratio, the vacancies.

Atomizing, mechanical milling/alloying, and self-propagating high-temperature sintering (SHS) are the most common manufacturing processes to produce intermetallic powders. Senderowski et al. [33] have recently worked on a new a concept of powder manufacturing based on the self-decomposition of the Fe-Al alloys, with the purpose of reducing the brittleness that is caused by dynamic oxidation at high temperatures (especially above 500 °C) in atmospheres containing oxygen. It was assumed that those powders would present sufficient plasticity for the spraying process, acceptable mechanical properties of the coatings, and good stability of the structure at high temperatures.

Including all of the previous considerations, the present work is intended to explore the high temperature sliding wear performance of several HVOF iron aluminide coatings of different nominal powder compositions, obtained through the previously mentioned manufacturing routes.

2. Experimental Procedure

The nominal composition and characteristics of the powders used in the study are presented in Table 1; the commercial FeAl Grade 3 atomized + ball milled powder of nearly equiatomic composition was provided by Mecachrome (Sablé-sur-Sarthe, France). The rest are experimental compositions that are obtained by the self-decomposition and self-propagating high-temperature sintering procedures at the University of Warmia and Mazury (Olsztyn, Poland). These powders were deposited onto low alloyed carbon steel substrate. The presence of boron in powder 1 may further improve material ductility and grain boundary cohesive strength [2,34], while Zr provides high-temperature strength through the solid solution [2,34].

Table 1. Iron aluminide feedstock powders.

Powder Nomenclature	Nominal Composition	Particle Size (μm)	Obtaining Procedure
Powder 1 (FeAl Grade 3)	Fe-40Al-0.05Zr (at.%) + 50 ppm B + 1 wt.% Y_2O_3	<50	Atomising + Ball milling
Powder 2	Fe-46Al-6.55Si (at.%)	<40	self-decomposed
Powder 3	Fe_xAl_y	−53 + 38	SHS multi-phases Fe_xAl_y type powder

The equipment used for the spraying process was the Diamond Jet Hybrid (DJH2700) from SULZER METCO (Winterthur, Switzerland). A low carbon steel was used as the substrate and the following spraying parameters were applied: O_2/H_2 fuel ratio = 0.301, feeding rate = 20 g·min^{-1}, spraying distance = 250 mm, traverse gun speed = 500 mm·s^{-1} and number of layers = 9. In addition, the samples were cooled with compressed air during the spraying process. Nitrogen was used as the powder carrying and shielding gas.

The coatings were properly degreased in acetone and afterwards mounted and polished. A SEM JEOL 5310 microscope (JEOL Ltd., Tokyo, Japan) was used to perform microstructural observation of the feedstock powder, coatings cross sections, and the worn-out surface of the wear tracks. The backscattered images were obtained with a K. E. Developments detector (K. E. Developments Ltd., Cambridge, UK). Qualitative microanalysis was performed by EDS with a RÖNTEC detector (Röntec, Berlin, Germany).

X-ray diffraction was used to analyze the phases in the feedstock powders and the sprayed coatings. All of the measurements were done using a Bragg-Brentano θ/2θ Siemens D-500 diffractometer with Cu Kα radiation (Siemens, Munich, Germany).

The Vickers microhardness was measured using a MATSUZAWA MXT-α indentation tester (Matsuzawa Co., Ltd., Akita, Japan) by applying a load of 200 gf for 15 s in the cross sections. Minimum 20 indentations were evaluated.

A sliding friction was tested with a ball-on-disc configuration by means of a CETR UMT-2MT universal mechanical tester (Bruker, Billerica, MA, USA) at 800 °C, with a heating rate of 18 °C min^{-1}. A 3.17 mm diameter Si_3N_4 ball was sliding down the polished coating surface (R_a < 0.8 μm). The test coated samples were of 25 mm × 25 mm × 5 mm dimensions. The sliding speed was set at 0.1 m·s^{-1}, the track diameter 4 mm and the sliding distance of 200 m were constant for all of the tests. Two tests per set conditions were carried out. The coefficient of friction was recorded along sliding distance at a normal load of 5 N. A brand new ball was used with every sample. Samples were cleaned using ultrasonic cleaner for 5 min and then dried. After mounting, both the sample and the ball were wiped using alcohol.

Given to the good results that will be presented for the as-sprayed FeAl Grade 3 powder, this was additionally tested at an intermediate temperature of 400 °C.

A Leica DCM3D confocal microscope (Leica Microsystems, Wetzlar, Germany) was used to obtain the wear track profiles so the volume loss could be found based on an extrapolation of a mean value of five cross sections. Depths up to 100 μm, with 0.1 nm resolution, and 0.3 nm RMS repeatability were represented independently of the magnification; lateral resolution was 500 nm.

The wear rate K (mm^3 N^{-1} m^{-1}) is calculated as:

$$K = \frac{V}{w \cdot s} \quad (1)$$

where V is the worn volume, w (N) is the normal load and s (m) is the total distance.

3. Results and Discussion

3.1. Powder Deposition

Figure 1 shows the particle size distribution of the feedstock powders. It can be observed that the prealloyed composition (powder 1) was characterized by the normal distribution that was centred at a mean size of 30 µm. On the contrary, the experimental self-decomposed and SHS powders were of non-symmetrical distribution. Powders 2 and 3 contained a larger amount of fine particles with $d10$ = 3 µm/$d90$ = 56 µm and $d10$ = 7 µm/$d90$ = 68 µm. The flowability of powders 2 and 3 was quite low.

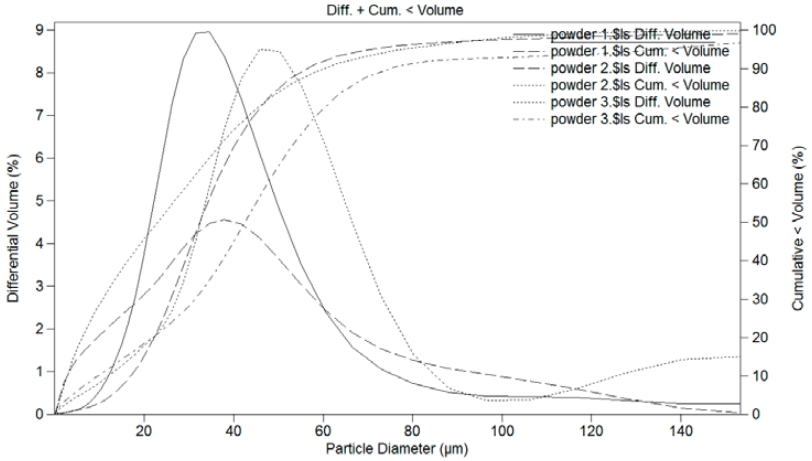

Figure 1. Particle size distribution of powders 1, 2, and 3.

Each of the three powders revealed an irregular morphology. The BSE-SEM micrographs of the cross sections showed the uniform composition of powder 1, whereas the other two presented the varied degree of greyness (Figure 2); the distribution of the phases in powders 2 and 3 from one particle to the other was considerably different (Figure 2b,c), especially in the last one, where some particles exhibited a laminar structure.

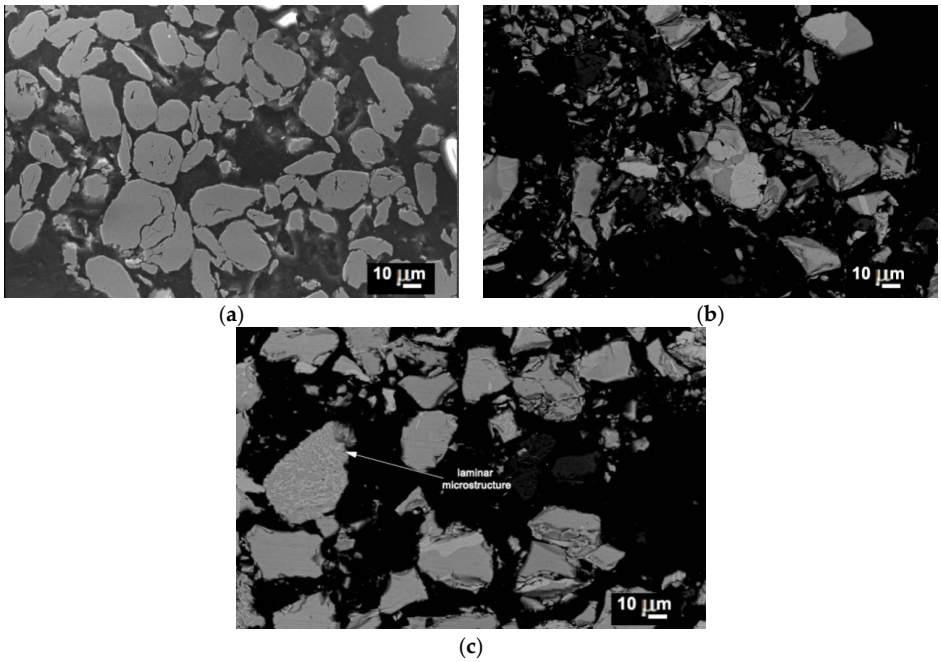

Figure 2. Cross sections of: (**a**) powder 1, (**b**) powder 2, and (**c**) powder 3.

Figure 3 shows the XRD of the powders. The peaks of powder 1 were identified as the fundamental lines of the FeAl intermetallic ($h + k + l$ = even), which appeared in the disordered lattice; no superlattice lines ($h + k + l$ = odd) were observed. The occurrence of broad peaks was related to the fine grain size and microstrains resulting from the milling. Powder 2 showed the presence of different intermetallic Fe-Al phases, mainly Fe_2Al_5 and $FeAl_3$, together with some SiO_2, while powder 3 contained FeAl, $FeAl_2$, Fe_2Al_5, and $FeAl_2O_4$. In [35], the self-decomposing process was analyzed in detail; these authors put forward a hypothesis about the self-decomposition of the Fe-Al-C-Me alloys (Me = Ni, Mn, Cr, Mo, V, B, Si). The powder was composed of iron aluminide intermetallic base with different Al content and thin oxide films as particle shells; this allowed for the obtainment of nanocomposite coatings.

From each powder, the same coatings were deposited. Figure 3 shows the as-sprayed cross sections of the powders 1, 2, and 3, with 103 ± 9, 76 ± 13 and 93 ± 11 µm of coating thickness respectively, after spraying nine layers. The coating obtained from the prealloyed powder (powder 1) was quite uniform in thickness whereas the other two were less homogeneous; the roughness of the coatings was found to be R_a = 3.06 ± 0.6, 4.3 ± 0.3, and 6.8 ± 0.4 µm, respectively.

The detailed inspection of the HVOF coating microstructures revealed the occurrence of the typical lamellar structure of thermal sprayed coatings with light and dark contrasts between splats and porosity (Figure 4). In coating 1 (Figure 4a), these were identified as iron-rich and oxide zones by EDS, respectively, and it was observed that heating the particles in-flight time resulted in the depletion of aluminium [36]. XRD confirmed the presence of oxidation (Figure 5); the additional peaks identified as FeAl corresponded to the superlattice lines in accordance with the ordering process when reaching the melting temperature [37].

The grey region in coating 2 consisted mainly of $FeAl_2$ and Fe_2Al_5, while the lightest phases at the intersplats were Fe-rich areas (Figure 4b). Some porosity was observed but not much oxidation, as detected in coating 1. In coating 3, the lightest regions were poorer in aluminium than the middle-grey ones that were identified by the Fe_3Al phase (Figure 4c).

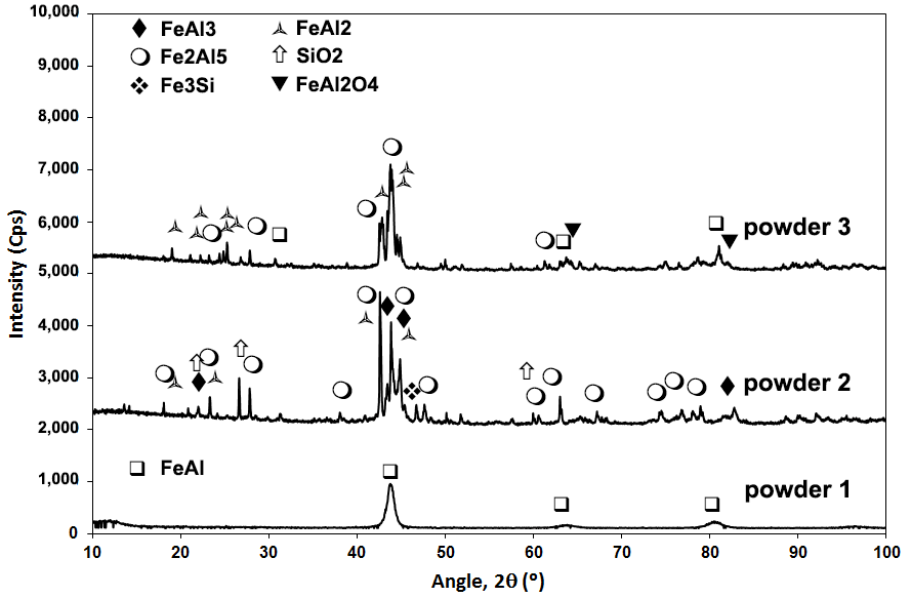

Figure 3. X-ray diffraction of the feedstock powders.

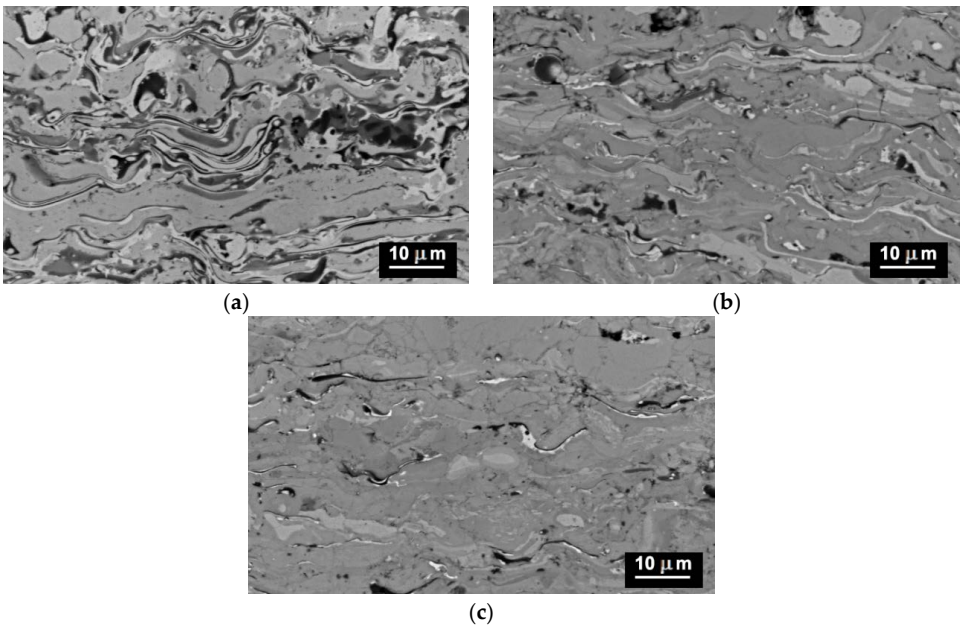

Figure 4. Cross sections of the FeAl coatings obtained with the different powders: (**a**) coating 1, (**b**) coating 2, and (**c**) coating 3.

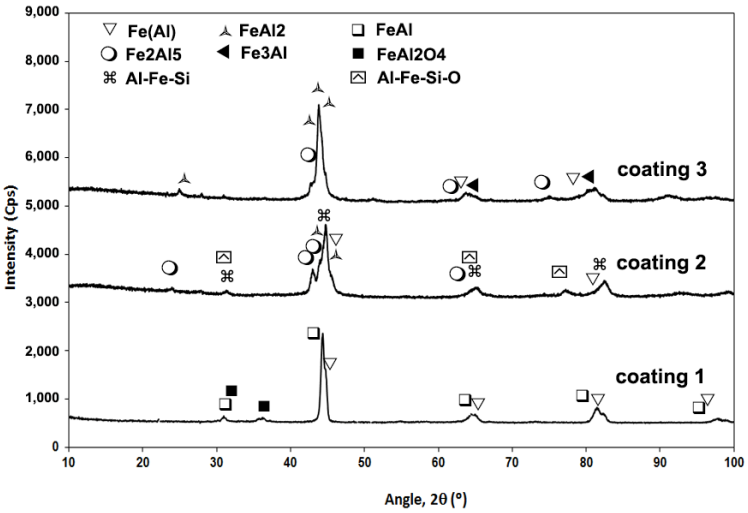

Figure 5. X-ray diffraction of the as-sprayed coatings.

The heterogeneous structure in the sprayed coatings may affect different properties, i.e., the occurrence of Al-depleted regions may lead to susceptibility to corrosion or oxidation and intersplat oxides may result in an increase of coating hardness and wear resistance; all of these features can be controlled by process variables i.e., spraying distance, oxygen and fuel flow rates, and particle size.

3.2. Coatings Performance

As it can be observed in Table 2, the microhardness values of coatings 1 and 2 are quite similar despite exhibiting different porosity levels, while the properties of coating 3 differ significantly, displaying a lower value due to its higher porosity and the amount of cracks in the as-sprayed condition. Actually, Figure 6 shows two indentations that were made in coatings 2 and 3 and illustrates the occurrence of many cracks as the result of applied force. It was observed that some of these cracks

propagated along the intersplat boundaries and can be explained by the embrittlement caused by the occurrence of the Al-rich phases, namely Fe_2Al_5 and $FeAl_2$ [38].

Table 2. Coating hardness values.

Coating Nomenclature	HV 0.2
Coating 1	505 ± 28
Coating 2	502 ± 35
Coating 3	423 ± 39

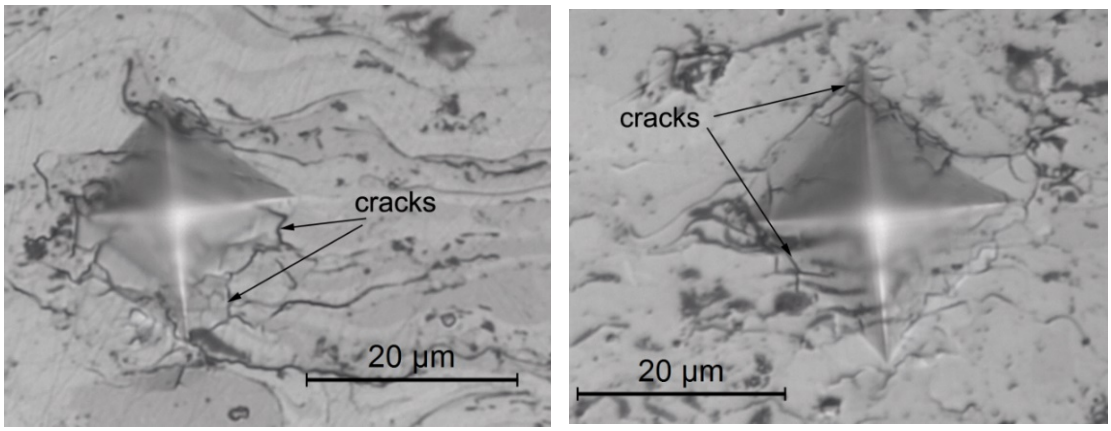

(**a**) (**b**)

Figure 6. Cracks formed at the indentations of (**a**) coating 2 and (**b**) coating 3.

In many cases, the hardness values were essential to predict the wear trend among different materials, according to Archard's equation [39], but it was also related to the characterized type of wear; therefore, when performing such an analysis, caution must be taken. By this mean, the abrasive performance can be predicted more accurately than sliding wear when hardness is taken into consideration. In addition, at high temperatures, the damage was increased due to the additional oxidation effect [40]. Figure 7 presents the XRD of the samples after the wear tests at 800 °C, showing the oxide products beside the wear tracks. For coatings 1 and 3, the formation of the fast growing oxide Fe_2O_3 at 800 °C, was observed; coating 2, however, showed similar phases as under the sprayed conditions, but with narrower peaks, which might be attributed to grain growth.

Figure 8 shows the variation of friction coefficient versus sliding distance at a normal load rate of 5 N for the different coating systems as well. It is was found that the friction coefficients fluctuate, which is probably due to plowing/delamination/oxidation mechanisms [12,32]; observations from Zhang et al. [12] are in agreement with that. Coating 1 presented a similar final COF as coating 3, while coating 2 peaked at a higher value; in addition, coating 1's curve was in fact quite smooth compared to coating 3, which presented ups and downs along the test; coating 2 however, started decreasing and then progressively increased afterwards, reaching a more stable value during the last few meters of the test.

The high initial values and the immediate drop can be attributed to the asperity contact given by the increased surface roughness initiated by oxide nodules. Coatings 1 and 3 tested at 800 °C, both formed Fe_2O_3 nodules (Figures 7 and 9), but the wear rates that were observed in Table 3 were quite different, i.e., negligible in coating 1 and high for coating 3. Given the positives tests of coating 1, this was also examined at 400 °C and proved a higher friction coefficient than at 800 °C, convergent with what was found at room temperature [31]. Such differences clearly indicated a transition of friction regimes at both temperatures influenced by the predominance of different wear mechanisms. Zhu et al. [41] reported a decrease of wear rate of undoped Fe-40Al with increasing temperature up to

500 °C. Other authors have reported that more rapid oxidation at 800 °C than at 400 °C may stabilize the adhesion of the oxide layer reducing friction [42].

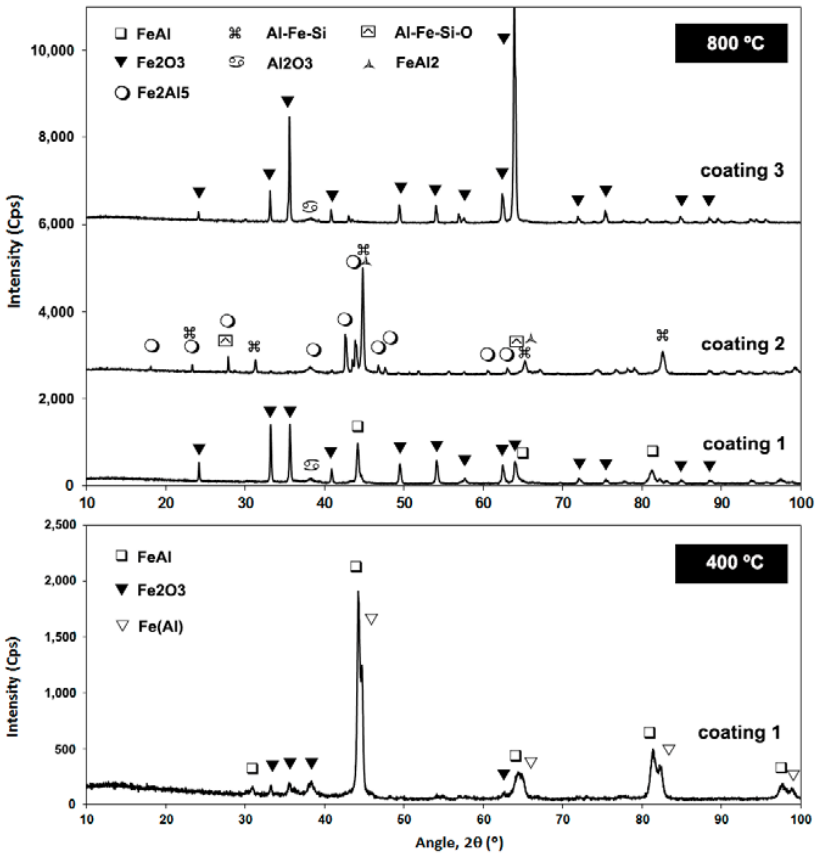

Figure 7. X-ray diffraction of the coating surfaces after the sliding wear test at moderate and high temperature.

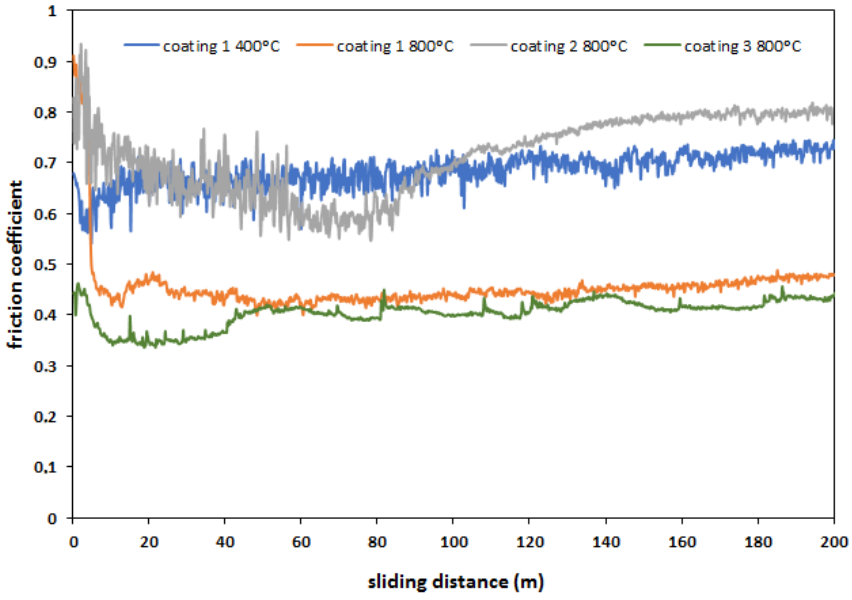

Figure 8. Coefficients of friction versus sliding distance of samples tested.

At 800 °C, the removal of oxide through sliding contact and reoxidation in coatings 1 and 3 was rapid enough to avoid Fe_2O_3 detachment as debris particles; it was also assumed that splat cohesion in coating 1 was good enough to prevent delamination mechanisms, which explained its low wear rate. Nevertheless, the presence of brittle Fe_2Al_5 and $FeAl_2$ phases in sprayed coating 3 might induce subsurface crack nucleation and fatigue mechanisms that would result in accelerated delamination. Coating 2 originally showed the presence of the Al-rich intermetallic phases, but the oxidation was much less extensive, and, although the same phases were identified at 800 °C, the friction coefficients followed different trends.

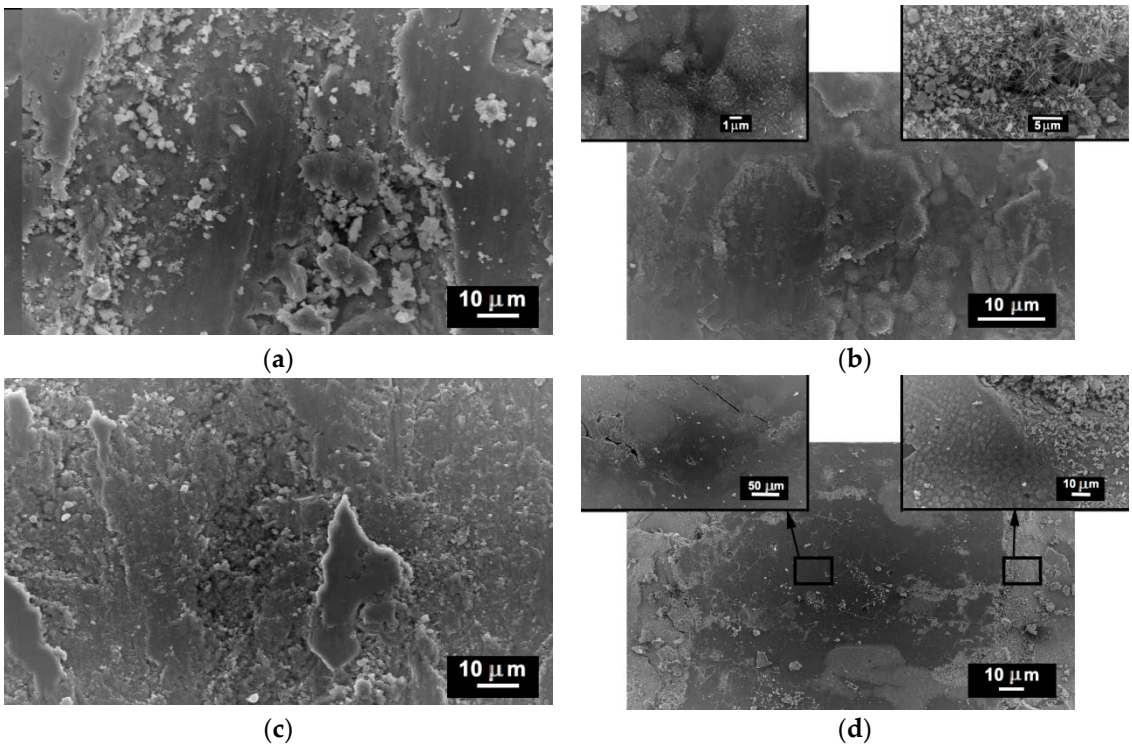

Figure 9. Wear debris after the ball-on-disk tests: (**a**) coating 1—400 °C, (**b**) coating 1—800 °C, (**c**) coating 2—800 °C, and (**d**) coating 3—800 °C.

Not only was the mean average of the friction coefficient value presented in Table 3, but also the value of wear tracks widths, depths and wear rates. Coating 1 displayed the lowest rates at both tested temperatures. The higher wear at 400 °C when compared to 800 °C was in agreement to the highest friction rate and might be attributed to the particulate adhesive wear debris observed during the examination of the wear track that remained between the contacting surfaces during sliding (Figure 9a) [12]. Additionally, the two-dimensional (2D) profiles of the wear tracks presented in Figure 10 confirmed the smoothness of the wear track of the coating tested at 800 °C; the roughness profile was indicative of the oxide layer formation.

Table 3. Mean values of coefficient of friction, wear track width and depth and wear rates.

Coating Nomenclature	*T* (°C)	Friction Coefficient	Wear Track Width (µm)	Wear Track Depth (µm)	Wear Rate ($mm^3\ N^{-1}\ m^{-1}$)
Coating 1	400	0.72 ± 0.06	625 ± 38	7.1 ± 0.1	$2.11 \times 10^{-5} \pm 2.00 \times 10^{-6}$
Coating 1	800	0.47 ± 0.05	480 ± 15	–	–
Coating 2	800	0.8 ± 0.13	1021 ± 30	48.5 ± 7.06	$4.67 \times 10^{-4} \pm 5.02 \times 10^{-5}$
Coating 3	800	0.43 ± 0.05	1399 ± 60	49	$3.87 \times 10^{-4} \pm 1.68 \times 10^{-4}$

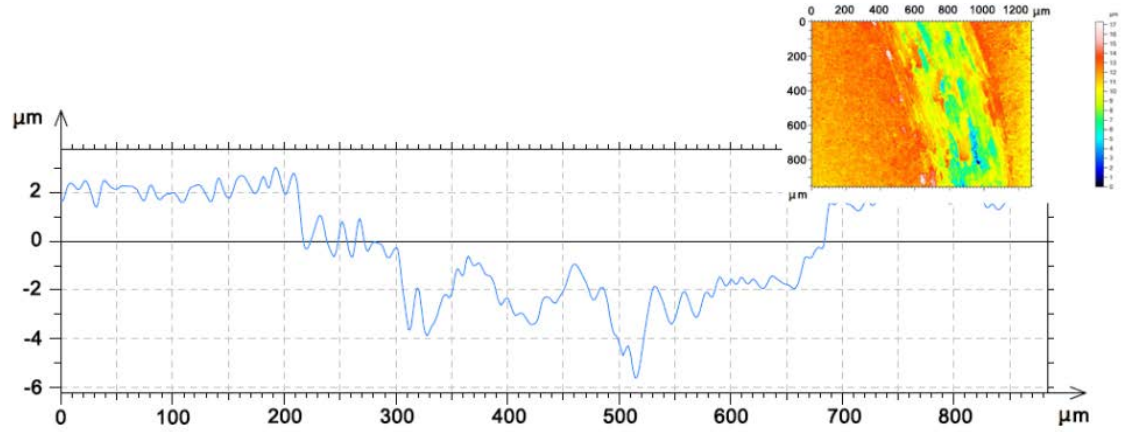

(**a**)

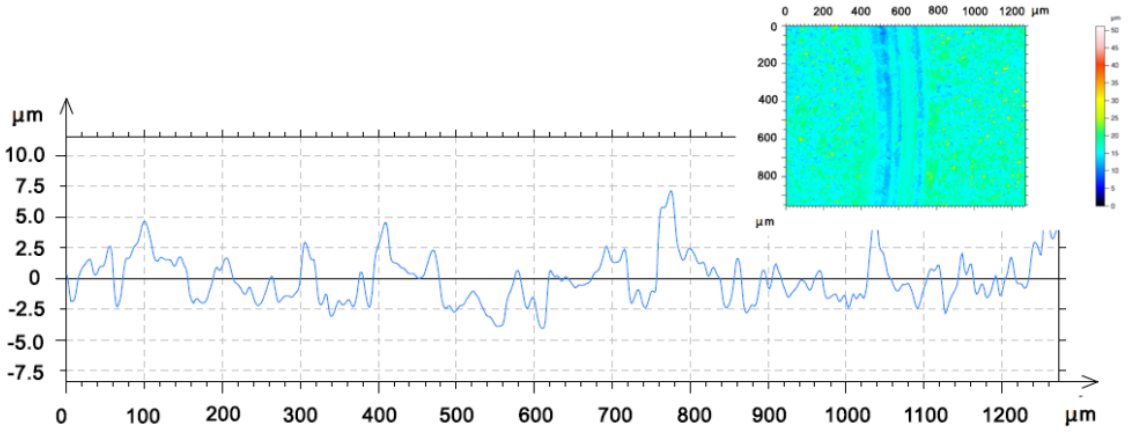

(**b**)

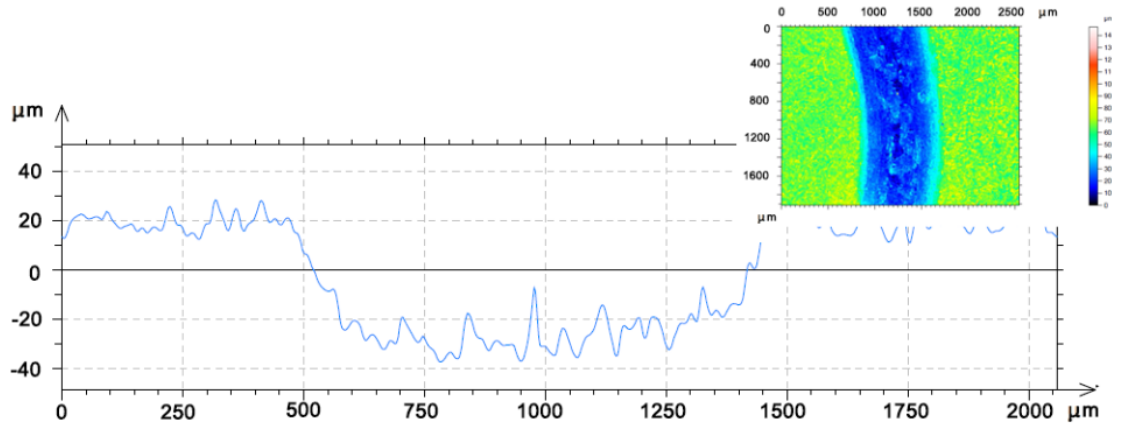

(**c**)

Figure 10. *Cont.*

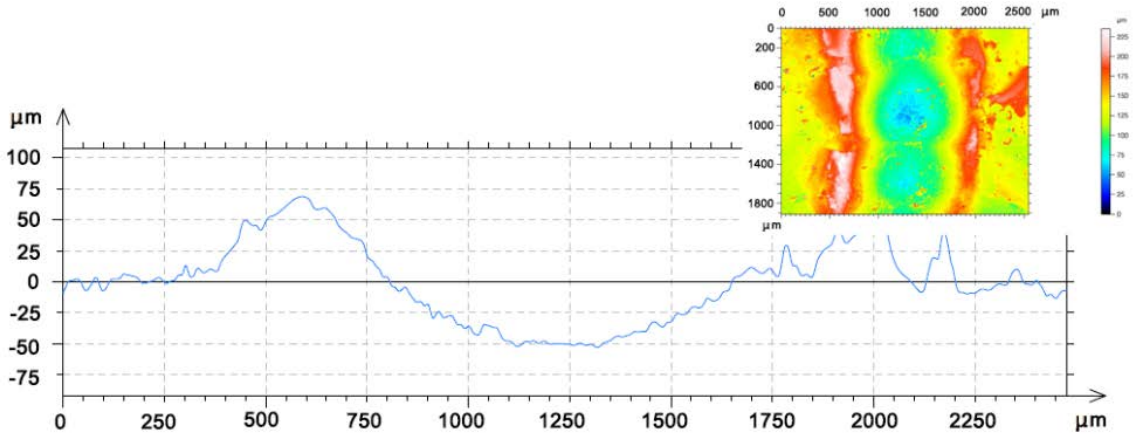

(**d**)

Figure 10. 2D wear track profiles of the FeAl coatings with respective colored topographic maps as insets: (**a**) coating 1—400 °C; (**b**) coating 1—800 °C; (**c**) coating 2—800 °C; and, (**d**) coating 3—800 °C.

Coating 1 showed better wear rates than high velocity arc sprayed (HVAS) coatings tested at room temperature by Xu et al. at 7 N, with a Si_3N_4 ball (55.4×10^{-5} $mm^3 \cdot m^{-1}$/7 N = 7.91×10^{-5} mm^3 N^{-1} m^{-1}) [26]. After the examination of the wear tracks, at 800 °C, coating 1 presented small Fe_2O_3 nodules formed by continuous oxidation of the freshly deposited coating (top left inset in Figure 9b); the top right inset showed the morphology of the oxidized surface with iron oxide nodules and needles. Coating 2 showed severe wear with patches of delaminated coating (Figure 9c). Coating 3, however, was formed by patches of fresh and oxidized coating (Figure 9d). The wear mechanism of coating 3 at 800 °C consisted of continuous formation and removal of a thick "glaze" tribofilm that was formed by smearing and sintering of iron oxide debris on the sliding surface. The high testing temperature was sufficient to promote the occurrence of such a dense glaze layer without the additional flash temperature between contacting surfaces.

The high wear rates at 800 °C of coatings 2 and 3 stemmed from the larger contact area, created by the lack of splat cohesion; the reported nanocomposite features that were reported by Senderowski et al. [38] did not seem to positively impact the wear performance. Moreover, it was proved that low intersplat cohesion favored oxygen penetration, which weakened the boundaries. The failure in coating 3 is well illustrated in Figure 11 through the cross section of the wear track, where the substrate was reached; this is in agreement to the predominance of iron oxide in the XRD analysis and the formation of the tribofilm layer, although both of the coating compositions were quite different, the performance appeared to be related to the microstructure, occurrence of brittle phases, subsequent delamination, and rapid oxidation. Other microstructural heterogeneities within the coating, such as pores, intersplat oxides, and other imperfections serve performed as stress concentrators. This lead to favorable conditions for crack initiation.

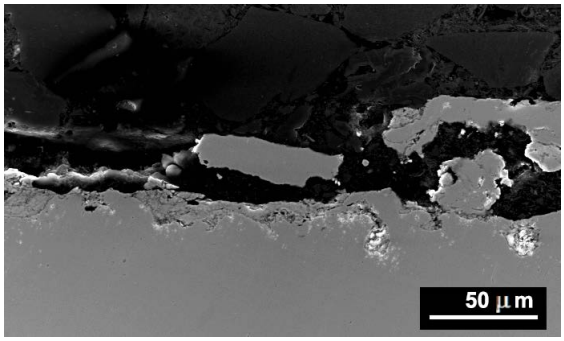

Figure 11. Cross section after the ball-on-disk tests for coating 3 at 800 °C.

4. Conclusions

The results of the present work can be summarised as follows:

- The coating hardness of the sprayed coatings 1 and 2 proved to be very similar, despite their different composition and original powder; this can be explained by heterogeneous balance in the HVOF coating, resulting from the presence of oxide regions as well as Al-depleted regions. The lowest hardness of the sprayed SHS powder came from the higher porosity levels.
- The self-decomposed and SHS feedstock compositions presented quite brittle phases that were detrimental to wear performance, enabling further penetration of the oxidizing atmosphere, even up to the point that coating 3 finally formed a dense tribofilm (glaze) layer. Delamination and tribo-oxidation were mainly identified as wear mechanisms that resulted from poor substrate cohesion.
- Wear rates for coating 1 were in the order of $2.11 \times 10^{-5} \pm 2.00 \times 10^{-6}$ mm^3 N^{-1} m^{-1} at 400 °C and even lower at 800 °C, where the exact value could not be measured. The other coatings showed wear rates at one order of magnitude higher. The different performance appeared to be related to the microstructural features of the initial composition and the exposure to high temperatures. Cohesive strength in coating 1 as well as its effectiveness in forming a protective layer allowed for the suppression of delamination.

Author Contributions: Conceptualization, N.C. and L.J.; Methodology, S.C. and S.D.; Software, N.C.; Validation, L.J. and J.M.G.; Formal Analysis, N.C.; Investigation, N.C. and S.C.; Resources, S.D., C.S. and L.J.; Data Curation, N.C.; Writing—Original Draft Preparation, N.C.; Writing—Review & Editing, N.C., S.C., C.S. and J.M.G; Visualization, I.G.C.; Supervision, J.M.G. and L.J.; Project Administration, J.M.G.; Funding Acquisition, J.M.G., C.S. and L.J.

Funding: The research was funded by the People Programme (Accions Marie Curie) of the 7 Framework Programme of the European Union (FP7/2007-2013) under REA grant agreement no. 600388 (TECNIOspring programme), and the Agency for Business Competitiveness of the Government of Catalonia, ACCIÓ.

Acknowledgments: We acknowledge the Centres Cientificotècnics from University of Barcelona for the technical support on XRD measurements.

Conflicts of Interest: The authors declare no conflict of interest.

References

1. Fleischer, R.L.; Dimiduk, D.M.; Lipsitt, H.A. Intermetallic compounds for strong high temperature materials: Status and potential. *Annu. Rev. Mater. Sci.* **1989**, *19*, 231–253. [CrossRef]
2. Deevi, S.C.; Sikka, V.K.; Liu, C.T. Processing, properties and applications of nickel and iron aluminides. *Prog. Mater. Sci.* **1997**, *42*, 177–192. [CrossRef]
3. Deevi, S.C.; Sikka, V.K. Nickel and iron aluminides: An overview on properties, processing, and applications. *Intermetallics* **1996**, *4*, 357–375. [CrossRef]
4. Guan, X.; Iwasaki, K.; Kishi, K.; Yamamoto, M.; Tanaka, R. Dry sliding wear behavior of Fe-28Al and Fe-28Al-10Ti alloys. *Mater. Sci. Eng. A* **2004**, *366*, 127–134. [CrossRef]
5. Sharma, G.; Limaye, P.K.; Ramanujan, R.V.; Sundararaman, M.; Prabhu, N. Dry-sliding wear studies of Fe_3Al-ordered intermetallic alloy. *Mater. Sci. Eng. A* **2004**, *386*, 408–414. [CrossRef]
6. Johnson, B.J.; Kennedy, F.E.; Baker, I. Dry Sliding Wear of NiAl. *Wear* **1996**, *192*, 241–247. [CrossRef]
7. Gong, K. A Ni3Al-alloy and Its Composites as Potential Wear Resistant Materials for Advanced Applications. Ph.D. Thesis, Chalmers University of Technology, Gothenburg, Sweden, 28 October 2011.
8. Hawk, J.A.; Alman, D.E. Abrasive wear of intermetallic-based alloys and composites. *Mater. Sci. Eng. A* **1997**, *239*, 899–906. [CrossRef]
9. Alman, D.E.; Hawk, J.A.; Tylczak, J.H.; Dogan, C.P.; Wilson, R.D. Wear of iron-aluminide intermetallic-based alloys and composites by hard particles. *Wear* **2001**, *251*, 875–884. [CrossRef]
10. Subramanian, R.; Schneibel, J.H. FeAl-TiC and FeAl-WC composites—Melt infiltration processing, microstructure and mechanical properties. *Mater. Sci. Eng. A* **1998**, *244*, 103–112. [CrossRef]
11. Ahmadian, M.; Wexler, D.; Chandra, T.; Calka, A. Abrasive wear of WC-FeAl-B and WC-Ni_3Al-B composites. *Int. J. Refract. Met. Hard Mater.* **2005**, *23*, 155–159. [CrossRef]

12. Zhang, X.; Ma, J.; Fu, L.; Zhu, S.; Li, F.; Yang, J.; Liu, W. High temperature wear resistance of Fe–28Al–5Cr alloy and its composites reinforced by TiC. *Tribol. Int.* **2013**, *61*, 48–55. [CrossRef]
13. Mosbah, A.Y.; Wexler, D.; Calka, A. Abrasive wear of WC-FeAl composites. *Wear* **2005**, *258*, 1337–1341. [CrossRef]
14. Qiu, J.; Baker, I.; Kennedy, F.E.; Liu, Y.; Munroe, P.R. The effects of stoichiometry on the dry sliding wear of FeAl. *Intermetallics* **2013**, *40*, 19–27. [CrossRef]
15. Roy, M. The influence of temperature on the wear of Cr_3C_2−25(Ni20Cr) coating-comparison between nanocrystalline grains and conventional grains. *Wear* **2004**, *257*, 799–811. [CrossRef]
16. Taktak, S. Tribological behaviour of borided bearing steels at elevated temperatures. *Surf. Coat. Technol.* **2006**, *201*, 2230–2239. [CrossRef]
17. Morris, D.G.; Muñoz-Morris, M.A. Intermetallics: Past, present and future. *Rev. Metal.* **2005**, *41*, 498–501. [CrossRef]
18. Lasalmonie, A. Intermetallics: Why is it so difficult to introduce them in gas turbine engines? *Intermetallics* **2006**, *14*, 1123–1129. [CrossRef]
19. Suryanarayana, C. Mechanical alloying and milling. *Prog. Mater. Sci.* **2001**, *46*, 1–184. [CrossRef]
20. Haghighi, S.E.; Janghorban, K.; Izadi, S. Order-sintering of mechanically alloyed FeAl nanostructures. *J. Alloys Compd.* **2010**, *503*, 375–379. [CrossRef]
21. Wang, B.; Lee, S.W. Erosion-corrosion behaviour of HVOF NiAl-Al_2O_3 intermetallic-ceramic coating. *Wear* **2000**, *239*, 83–90. [CrossRef]
22. Zhang, J.; Sun, K.; Wang, J.; Tian, B.; Wang, H.; Yin, Y. Sliding wear behavior of plasma sprayed Fe_3Al-Al_2O_3 graded coatings. *Thin Solid Films* **2008**, *516*, 5681–5685. [CrossRef]
23. Wang, Y.; Yan, M. The effect of CeO_2 on the erosion and abrasive wear of thermal sprayed FeAl intermetallic alloy coatings. *Wear* **2006**, *261*, 1201–1207. [CrossRef]
24. Hearley, J.A.; Little, J.A.; Sturgeon, A.J. The erosion behaviour of NiAl intermetallic coatings produced by high velocity oxy-fuel thermal spraying. *Wear* **1999**, *233*, 328–333. [CrossRef]
25. Cinca, N.; Guilemany, J.M. Thermal spraying of transition metal aluminides: An overview. *Intermetallics* **2012**, *24*, 60–72. [CrossRef]
26. Xu, B.; Zhu, Z.; Ma, S.; Zhang, W.; Liu, W. Sliding wear behavior of FeAl and FeAl/WC coatings prepared by high velocity arc spraying. *Wear* **2004**, *257*, 1089–1095. [CrossRef]
27. Tian, B.-H.; Liu, P.; Xu, B.S.; Ma, S.-N.; Zhang, W.; Li, S.Z. Tribological properties of thermal spray formed Fe_3Al-based coatings at elevated temperature. *Chin. J. Nonferr. Met.* **2003**, *13*, 974–978. (In Chinese)
28. Amiriyan, M.; Blais, C.; Savoie, S.; Schulz, R.; Gariépy, M.; Alamdari, H. Tribo-Mechanical Properties of HVOF Deposited Fe_3Al Coatings Reinforced with TiB_2 Particles for Wear-Resistant Applications. *Materials* **2016**, *9*, 117. [CrossRef] [PubMed]
29. Vinush, G.; Achutha, M.V.; Rakash, K.R. Dry Sliding Wear Behaviour of Nickel Aluminide coated on Zinc Aluminium alloy Metal Matrix Composite for Anti friction Applications. *Int. J. Curr. Eng. Technol.* **2015**, *5*, 1836–1840.
30. Wang, Y.; Chen, W.; Wang, L. Micro-Indentation and Erosion Properties of Thermal Sprayed NiAl Intermetallic-Based Alloy Coatings. *Wear* **2003**, *254*, 350–355. [CrossRef]
31. Guilemany, J.M.; Cinca, N.; Fernandez, J.; Sampath, S. Erosion, abrasive, and Friction Wear Behavior of Iron Aluminide Coatings Sprayed by HVOF. *J. Therm. Spray Technol.* **2008**, *17*, 762–773. [CrossRef]
32. Zamanzade, M.; Barnoush, A.; Christian, M. A review on the Properties of Iron Aluminide Intermetallics. *Crystals* **2016**, *6*, 10. [CrossRef]
33. Senderowski, C.; Zasada, D.; Durejko, T.; Bojar, Z. Characterization of as-synthesized and mechanically milled Fe–Al powders produced by the self-disintegration method. *Powder Technol.* **2014**, *263*, 96–103. [CrossRef]
34. McKamey, C.G.; DeVan, J.H.; Tortorelli, P.F.; Sikka, V.K. A review of recent developments in Fe_3Al-based alloys. *J. Mater. Res.* **1991**, *6*, 1779–1805. [CrossRef]
35. Sozańska, M.; Kościelniak, B.; Swadźba, L. Evaluation of Hot Corrosion Resistance of Directionally Solidified Nickel-Based Superalloy. *Solid State Phenom.* **2015**, *227*, 337–340. [CrossRef]
36. Guilemany, J.M.; Lima, C.R.C.; Cinca, N.; Miguel, J.R. Studies of Fe-40Al coatings obtained by high velocity oxy-fuel. *Surf. Coat. Technol.* **2006**, *201*, 2072–2079. [CrossRef]

37. Cinca, N.; Dosta, S.; Guilemany, J.M. Nanoscale characterization of FeAl-HVOF coatings. *Surf. Coat. Technol.* **2010**, *205*, 967–973. [CrossRef]
38. Senderowski, C.; Bojar, Z.; Wolczynski, W.; Pawlowski, A. Microstructure characterization of D-gun sprayed Fe-Al intermetallic coatings. *Intermetallics* **2010**, *18*, 1405–1409. [CrossRef]
39. Hutchings, I.; Shipway, P. *Tribology: Friction and Wear of Engineering Materials*, 2nd ed.; Elsevier: Oxford, UK, 2017; ISBN 9780081009109.
40. Pauschitz, A.; Roy, M.; Franek, F. Mechanisms of sliding wear of metals and alloys at elevated temperatures. *Tribol. Int.* **2008**, *41*, 584–602. [CrossRef]
41. Zhu, S.; Guan, X.; Shibata, K.; Iwasaki, K. Microstructure and mechanical and tribological properties of high carbon Fe_3Al and FeAl intermetallic alloys. *Mater. Trans.* **2002**, *43*, 36–41. [CrossRef]
42. Sassatelli, P.; Bolelli, G.; Lassinantti Gualtieri, M.; Heinonen, E.; Honkanen, M.; Lusvarghi, L.; Manfredini, T.; Rigone, R.; Vippola, M. Properties of HVOF-sprayed Stellite-6 coatings. *Surf. Coat. Techol.* **2018**, *338*, 45–62. [CrossRef]